

ALMA Memo 351

March 2001

**275-370 GHz DSB and SSB waveguide mixers employing
a tuned Nb/Al-AIO_x/Nb SIS tunnel junction**

A. Navarrini and B. Lazareff

(navarrin@iram.fr ; lazareff@iram.fr)

IRAM (Institut de Radio Astronomie Millimétrique)

Domaine Universitaire

38406 St. Martin d'Hères

France

275-370 GHz DSB and SSB waveguide mixers employing a tuned Nb/Al-AIO_x/Nb SIS tunnel junction

A. Navarrini, B. Lazareff

Abstract

We discuss the design and optimisation of two full height waveguide SIS mixers for astronomical applications both covering the 275-370 GHz frequency band: a Double Side Band (DSB) and a Single Side Band (SSB) mixer. The expected SSB receiver noise temperature referred to the mixer input are in the range 23-35 K for the DSB and 25-38 K for SSB mixer. A $\approx 30\%$ operating bandwidth can be achieved in the DSB case by using an "end-loaded" tuning stub to tune out the junction capacitance of 75 fF (junction size $1 \mu\text{m}^2$) followed by two quarter-wave transformer sections. A similar operating bandwidth is obtained in the SSB mixer by using a parallel tuning inductor with a radial microstrip stub. Single junctions are mounted on a 80 μm thick quartz which stretches only part way across the waveguide. In the SSB mixer the image rejection is obtained using a mechanically rugged noncontacting backshort with a circular cross-section which can be moved inside a circular waveguide. Both mixers have a 4 GHz IF passband and a central IF frequency of 6 GHz. A stability criterion for intrinsically DSB and SSB mixers under typical operating conditions has been derived. We have shown that when an inductive series matching structure is used to compensate the junction capacitance, the SSB mixer cannot be operated over a wide frequency range in a stable way. An inductive parallel matching structure allows us to fulfil the necessary conditions of stability. Receiver performance has been optimised for both mixers in order to guarantee a low mixer noise temperature while maintaining adequate gain and stable operations over the whole frequency band of interest.

CONTENTS

I. Introduction	3	III. SSB mixer	
II. DSB mixer		A. Circular section backshort	13
A. Full height waveguide to suspended microstrip transition	3	B. SSB tuning	14
B. RF filter	5	C. Stability of SSB mixer	15
C. Stability of DSB mixer	6	D. RF matching circuit	16
D. RF matching circuit	7	E. Junction bias and IF matching circuit	17
E. Junction bias and IF matching circuit	9	F. Gain and mixer noise temperature	18
F. Gain and mixer noise temperature	10	G. Mixer block construction	20
G. Mixer block construction	12	IV. Conclusion	20
		Acknowledgements	20
		References	21

I. Introduction

Radioastronomical spectroscopy is the main driver for the development of low-noise heterodyne receivers in the mm and submm range. Thanks to progress in junction fabrication and circuit design, receivers based upon Nb/Al-AIO_x/Nb junctions now achieve noise temperatures only a few times the quantum limit between approximately 100 GHz and 1 THz. This is especially true when the noise is referred to the mixer input. However, in a practical implementation on a telescope, the losses associated with infrared filtering, local oscillator injection, telescope spillover and atmospheric attenuation all contribute to degrade the actual figure of merit for astronomical spectroscopy: SSB system noise temperature. Referring the system noise to the mixer input, it can be expressed in a simplified form as:

$$T_{SSB} = G_S^{-1} \cdot (T_{out} + T_{IF}) + (1 + G_I / G_S) \cdot T_{in}$$

where G_S and G_I are the coupled mixer gain in the signal and image band, T_{out} is the mixer noise temperature referred to its output, T_{IF} is the noise temperature of the IF amplifier and T_{in} is the input noise temperature including noise contributions from optics, spillover and sky. A first requirement is to cover the atmospheric transmission windows with a minimum number of distinct receivers; this is a driver for a wide tuning range of the mixer (and of the LO system). A second requirement is for stable operation to be achieved without critical tuning. Accordingly, the main goals in the present work are: wide RF tuning range, low noise and stable operation. For a typical ground-based receiver, the second term of the above equation is often dominating the sum. Its impact can be minimized by realizing an SSB mixer. The present report is organized as follows: in section II we describe the design of the DSB mixer; it includes a discussion of a full height waveguide to suspended

microstrip transition (II.A), and of a "hammer" type RF filter (II.B) which are common to the DSB and SSB mixer design; in section II.C we derive a stability criterion for a DSB mixer while in II.D we discuss the series inductive RF matching circuit; the junction bias and IF matching circuit are studied in section II.E; finally, the expected gain and noise temperature of the DSB mixer are calculated in section II.F, while the mixer block construction is discussed in section II.G.

In section III we present the SSB mixer: a circular cross-section backshort and a circular to rectangular waveguide tapering are discussed in III.A. The SSB tuning and the stability of SSB mixer are discussed in III.B and III.C respectively. In section III.D we present the parallel inductive RF matching circuit, while the junction bias and IF matching circuit of the SSB mixer are discussed in III.E. In section III.F we calculate the expected gain and mixer noise temperature. Finally, the mixer block construction is discussed in III.G.

II. DSB mixer

A. Full height waveguide to suspended microstrip transition

The 275-370 GHz mixer waveguide supports single TE₁₀ mode operation from 197 GHz to 394 GHz. To achieve a good match over the desired frequency band it is imperative that a probe impedance $Z_{ant}(v)$ is selected which can easily be tuned over the entire frequency range. A waveguide whose height is reduced relative to the normal b/a ratio is often used in SIS mixers to help achieve the impedance match between the waveguide and the junction. We found desirable to use a full-height waveguide ($b/a=1/2$) for two reasons : i) lower losses ; ii) easier fabrication. Yassin and Withington [1] give analytical results for the transition from a full height waveguide to a TEM port, that achieves a very good match to a real,

low impedance (20-50 Ω) over a full waveguide band, making it well suited for an SIS mixer. However, their results refer to an ideal probe fed by a TEM port of negligible dimensions located on the wall of the waveguide. In a practical implementation, the TEM transmission line has a finite cross-section and in our case consists of a microstrip line on a quartz substrate that is housed in a channel perpendicular to the waveguide. We have therefore performed electromagnetic simulations of probe configurations using the FDTD package CST Microwave Studio [2]. A first step was to determine the size and orientation of the quartz substrate and its associated channel. A suspended microstrip line with a choke structure provides a virtual ground at the waveguide wall for the microstrip. Besides the fundamental TEM mode, the suspended microstrip line can support higher order modes. For the typical geometries that we have investigated, the first such mode is an odd one having a cut-off frequency which falls in the middle of the RF band of interest. Rather than raising the cut-off frequency of that mode above the highest operating frequency by reducing the suspended microstrip line cross-section, with increased fabrication difficulties, we decided to place the substrate perpendicular, rather than parallel, to the waveguide axis (see Fig. 1). In that configuration, the first higher order mode of the suspended microstrip line is decoupled from the TE_{10} mode of the waveguide by symmetry. With our adopted dimensions for the substrate and channel (width = 250 μm , fused quartz substrate thickness = 80 μm , 100 μm air below, 50 μm air above), the next higher order mode (an even one) in the suspended microstrip line is supported above 495 GHz (for the widest strip¹), safely outside our operating range.

A second step was to optimise the antenna configuration. We found that the interaction

of the suspended microstrip line choke with the antenna-waveguide coupling is adequately taken into account when the numerical simulation includes only the first two sections of the choke, terminated to a

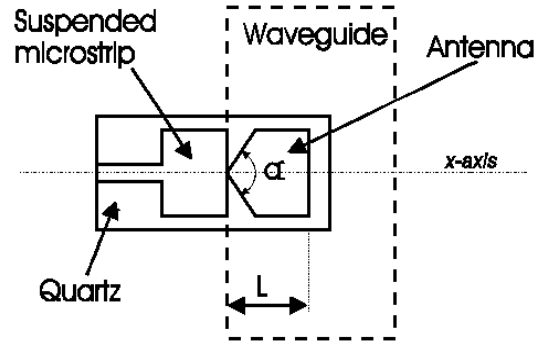


Fig. 1: Full height waveguide to suspended microstrip transition: the quartz substrate extends only part way across the waveguide. An antenna probe of length L and opening angle α has been optimised to have a low real impedance in a broad bandwidth.

short. The numerical simulation determines the driving point impedance between the base of the antenna and the centre of the edge of the choke for a distance between the antenna plane and a short circuit (located behind the quartz substrate) of approximately $\lambda_g/4$. We parameterised possible antenna geometries by two parameters: the length L of the antenna, and the opening angle α at the antenna apex. The quartz substrate was assumed to extend only a minimal amount (20 μm) beyond the tip of the antenna: a broader response can be achieved when the substrate does not extend beyond the antenna to the opposite waveguide wall. We find that over the design frequency range, the driving point impedance Z_{ant} remains in a small region of the Smith chart, and that, together, L and α control the real and imaginary part of the average impedance. Increasing L results in an increase of $\text{Re}(Z_{\text{ant}})$ and a decrease of $\text{Im}(Z_{\text{ant}})$, while increasing α results in a decrease of both $\text{Re}(Z_{\text{ant}})$ and $\text{Im}(Z_{\text{ant}})$. The results for two possible probes, having (at the center of the working frequency range)

¹ Wider strips have lower cut-off frequencies for higher order modes [3].

almost real impedance, are illustrated on Fig. 2. We can see that both types of probes are low impedance and broad bandwidth giving a real part of about 50Ω for antenna 1, and about 75Ω for antenna 2. This study has shown that wideband operations with low impedance levels can be obtained without a reduction in height of the waveguide by using a one-sided probe mounted on a suspended microstrip line.

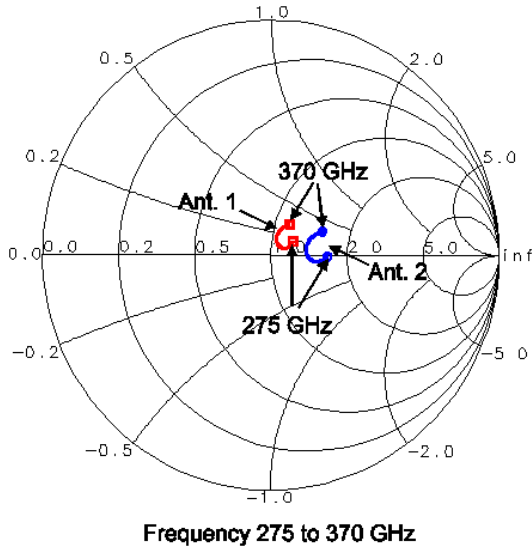


Fig. 2 : Input impedance for two different types of one-sided antenna probes mounted in a suspended microstrip line : Ant. 1 has a length $L = 188 \text{ mm}$ and an opening angle a of 130° ; Ant. 2 has a length $L = 200 \text{ mm}$ and an opening angle a of 90° . The Smith chart is normalised to 50Ω .

B. RF filter

A low pass "hammer" type filter in suspended microstrip line has been optimised to give maximum rejection in the 200-400 GHz frequency band. Figure 3 shows the six

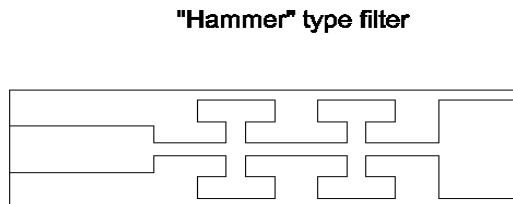


Fig. 3 : Six sections hammer type filter. A 50Ω line is added on the left part of the filter.

sections filter (plus a 50Ω line on the left) which is used to prevent the RF signal leakage in the substrate channel via the IF and DC connections to the junction. The performance of this filter has been compared with that of a (previously optimised) six sections ordinary low pass filter composed of alternating parts of transmission line with high and low characteristic impedance. In both types of filters the width of the high impedance lines (narrow strips) are equal.

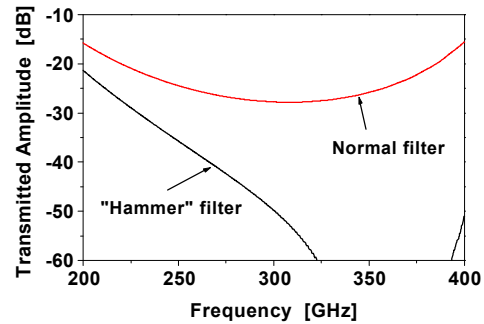


Fig. 4 : Amplitude of the transmission coefficient of six sections "Hammer" type and normal type filter as a function of frequency.

The geometry of the hammer sections have been optimised to give maximum rejection in the 275-370 GHz band. The advantage of the six sections hammer filter with respect to the six sections ordinary filter is significant, as can be seen in Fig. 4. The hammer filter shows superior performances in the whole band of interest.

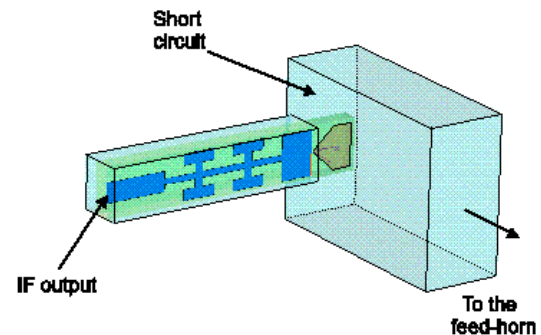


Fig. 5 : Three-dimensional view of the full height waveguide DSB mixer integrating the RF hammer type filter.

Fig. 5 shows a three-dimensional view of the mixer integrating the hammer filter and the antenna type 1.

C. Stability of DSB mixer

Tucker's theory of mixing [4] has been used to derive a stability criterion for a DSB mixer operating in the 275-370 GHz frequency range in the limit of low v_{IF} frequencies ($v_{IF}/v_{LO} \rightarrow 0$). Mixer properties are calculated using a three-port approximation which means that the currents generated at $v_m = v_{IF} + m v_{LO}$, $|m| \geq 2$ are assumed to be short circuited by the junction's geometrical capacitance. The IF output admittance Y_{IF} of a SIS mixer is given by :

$$Y_{IF} = \frac{1}{Z_{00}} - Y_I \quad (1)$$

where Z is the inverse of the augmented Y matrix (see Tucker and Feldmann [5] for details), and Y_I is the load admittance of the IF circuit. Although it is not obvious from the algebra, Y_{IF} depends on Y_{USB} and Y_{LSB} , the terminating admittances respectively at USB and LSB port, but not on Y_I ; this is what is expected intuitively since it represents the impedance seen at the IF port of the junction when the USB and LSB ports are terminated at definite impedances. Its value depends on the operating conditions of the pumped junction and on the impedance termination at the signal Z_S , and image band Z_I . Here the S and I subscript are used to indicate that the signal and image band can be either the USB or the LSB. In the limit $v_{IF} \rightarrow 0$, it can be shown that in a purely DSB mixer where $Z_S = Z_I^*$, $\text{Im}[Y_{IF}] = 0$ [6], while $\text{Re}[Y_{IF}]$ can become negative depending on the value of Z_S and on the adopted pumping conditions. In this case, Y_{IF} is also the slope of the pumped I-V characteristic for a fixed LO pumping power² at the given V_{DC} bias voltage. For our calculations we have assumed DSB operation

with $\text{Im}[Y_{IF}] = 0$. Negative resistance regions on the pumped I-V curve is a characteristic of mixers that operate in the quantum regime, while for classical resistive mixers the condition $Y_{IF} > 0$ is always verified. Any device with negative differential resistance is potentially unstable. In a SIS mixer this instability could cause oscillations in the RF, IF or bias circuit. The IF load admittance Y_I should then be carefully chosen in such a way that $Y_{IF} + \text{Re}[Y_I] > 0$, which is the condition to avoid oscillation. An alternative with better safety margins that we have adopted to guarantee stable operation is to design the DSB mixer by selecting $Z_S = Z_I^*$ and the operating conditions for the bias and pumping voltages so that $Y_{IF} > 0$ for a value of Z_S giving optimum receiver performances. Optimum operating conditions depend on many parameters and are discussed by L.R. D'Addario [7]. Here, we have assumed these conditions are achieved for a bias voltage V_{DC} at the half of the first photon step, $V_{DC} = V_g - hv_{LO}/2e$, (with $V_g \cong 2.8$ mV gap voltage for the Nb at 4 K, and e electron charge) where the conversion loss and noise are normally low, and for a LO pumping voltage parameter $\alpha = e \cdot v_{LO}/hv_{LO} = 1$. We have used a three-frequency approximation to the quantum theory of mixing to constrain all the possible values of $Z_S = Z_I^*$ necessary to obtain $Y_{IF} > 0$ at the centre of the RF frequency band, 322.5 GHz. This has been done by using an analytic fit to a good quality I-V curve of a measured junction characterised by a low sub-gap current. The result of this analysis are plotted in the Smith chart of Fig. 6. Each point of the chart represents the complex value of the RF embedding impedance $Z_{emb} = Z_S$. Tucker's theory has been applied for each impedance value in order to determine whether the value of Y_{IF} is positive or negative. The hatched part of the chart delimited by the dotted line represents the resulting impedance regions for which $Y_{IF} < 0$ at 322.5 GHz. We can see that the condition $Y_{IF} > 0$ is obtained for values of

² Fixed LO power does not in general correspond to fixed LO amplitude across the junction.

$Z_S = Z_I^*$ approximately located in the lower part of the Smith chart. Thus, optimum operating conditions and stable operations are achieved when the RF impedance seen by

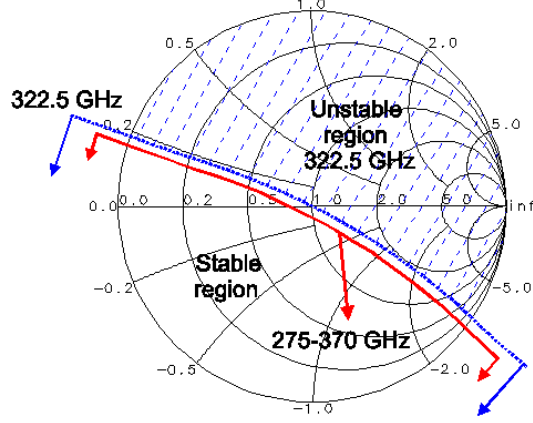


Fig. 6: "Stability regions" for a purely DSB mixer at 322.5 GHz (delimited by the blue line) and in the 275-370 GHz frequency band (delimited by the red line). The hatched part of the chart represents the region where the value of impedances $Z_S = Z_I^*$ are such that $\text{Re}[Y_{IF}] < 0$. The operating conditions $\alpha=1$ and $V_{DC} = V_g - \hbar n_{LO}/2e$ are used. The Smith chart is normalised to R_n .

the junction is slightly lower than its normal-state resistance R_n and capacitive. The study of the stability has been repeated for every possible Z_{emb} at each frequency in the range 275-370 GHz. We have found that the lower frequency of the RF band constrain the limits of the stability region in the whole band. The stable region in this frequency band is shown in the same Fig. 6 and is delimited by the solid line. The derived "stability criterion" has been used as a design rule to be fulfilled by the DSB mixer to guarantee stable operations.

D. RF matching circuit

At RF, the SIS tunnel junction is shorted out by the high value of its intrinsic capacitance C due to the two niobium films which are separated by a very thin ($\approx 10 \text{ \AA}$) insulator. The $1 \mu\text{m}^2$ Nb/Al-AIO_x/Nb junction has a critical current density of the order of 10 kA/cm^2 and a normal-state resistance $R_n = 25 \Omega$ [8]. It will be realised with e-beam

lithography process. The geometric capacitance of the junction is in parallel with the quantum reactance of the tunnel barrier. The susceptance B_{11} of the barrier is nearly zero for bias voltages on the first quasi-particle step, therefore its contribution can be neglected with respect to the susceptance due to the junction capacitance. The small-signal RF input conductance of a mixer is described by Tucker's quantum theory :

$$G_{11} = \frac{e}{2\hbar\omega} \cdot \sum J_n^2(\alpha) \cdot \left[I_{DC} \left(V_0 + \frac{(n+1)\hbar\omega}{e} \right) - I_{DC} \left(V_0 + \frac{(n-1)\hbar\omega}{e} \right) \right]$$

which for small values of α is given by the slope of a line joining points on the pumped I-V curve one photon step above and one photon step below the DC bias point. Thus, the real part of the impedance R_j presented by the mixer at the RF port is lower than the normal-state impedance R_n of the junction and of the order of $R_j \approx 0.66 \cdot R_n \approx 16.4 \Omega$ at 275 GHz and $R_j \approx 0.84 \cdot R_n \approx 20.9 \Omega$ at 370 GHz. Given the slow dependence of this RF resistance on the frequency, a value of $R_j \approx 0.75 \cdot R_n \approx 18.7 \Omega$ at the central frequency of 322.5 GHz has been assumed for design purposes. The corresponding $\omega R_j C$ product at this frequency is ≈ 2.8 . The RF impedance of the junction has then been approximated as an R_j resistance of 18.7Ω in parallel with a 75 fF capacitance. The RF junction impedance in parallel with its capacitance must be transformed to the value of the antenna probe impedance of $\approx 50 \Omega$ (antenna type 1 discussed in sec. II.A is used). The real part of the RF equivalent impedance of the junction in parallel with its capacitance, Z_0 , is very low and of the order of $\text{Re}[Z_0] \approx R_j / (\omega R_j C)^2 \approx 2.3 \Omega$. To improve the junction match to the embedding impedance and to increase the instantaneous bandwidth of the mixer, a variety of inductive tuning circuits have been introduced. The RF fractional bandwidth $B = \Delta\omega/\omega$ obtained

with such stub is proportional to $(\omega RC)^{-1}$. A common way to tune out the junction capacitance in a wide frequency band is using an end-loaded tuning circuit as discussed by several authors (see [9] for example). The end-loaded stub puts a small section transmission line in series with the junction. This results in the transformation of the complex junction impedance Z_0 to a purely real impedance R_s . The length l_s of the inductive transmission line of characteristic impedance $1/(\omega C)$ necessary to this transformation can be obtained from the following equation [10] :

$$\tan(\beta \cdot l_s) = \frac{1}{2 \omega^2 C^2} \cdot \left(\sqrt{\frac{1}{R_j^4} + \frac{4}{(\omega C)^4}} - \frac{1}{R_j^2} \right)$$

where $\beta = 2 \pi / \lambda$ is the propagation constant of the transmission line. For $\omega R_j C \gg 1$ an analytical approximation to the resistance R_s simplifies to :

$$R_s \approx \frac{R_j}{2 \cdot (\omega R_j C)^2}$$

The R_s value has then been transformed to the $\approx 50 \Omega$ antenna probe impedance by means of a two sections quarter-wave transformer. The inductive line and the first section of the quarter-wave transformer are implemented in superconducting microstrips. The second section of the quarter wave transformer (next to the antenna) cannot be realised as a single microstrip section because its required impedance is of the order of 30Ω . This is much higher than the highest 17Ω value which can be obtained with a width of the strip of $2 \mu\text{m}$ which is the lower technological limit for the width at IRAM. Therefore, the 30Ω line has been realised as a Capacitively Loaded Coplanar Waveguide (CLCPW). The CLCPW transmission line is made of a combination of two coplanar waveguide sections (CPW) interconnected via 3 microstrip sections. All the strips and their ground planes are made of Nb (120 nm and

430 nm respectively) separated by a 200 nm thick insulating layer of SiO_2 ($\epsilon_R \cong 4.3$). The widths and lengths of the inductive line and of the Chebyshev transformer have been optimised for maximum coupling of the RF junction resistance to the antenna probe in the 275-370 GHz frequency range, by using a commercial software (Series IV HP-EEsof Microwave & RF Design, Libra-Touchstone). However, Libra is unable to calculate superconducting parameters either for microstrip lines (using equations derived by Chang [11]) or coplanar waveguides. The use of superconducting lines instead of normal metal lines give rise to a decrease of the propagation speed and to an increase of the impedance of the lines. These effects are important when the London penetration depth λ_L in Nb (assumed to be 86 nm at 4 K) is of the same order of the distance between the 2 conductors. In the microstrip case, this distance corresponds to the thickness of the SiO_2 insulating layer (200 nm), while for the CPW this corresponds to the gap between central strip and the two external ground layers (which has been fixed to $4 \mu\text{m}$). Thus, superconducting effects were taken into account in the microstrip case, while they were neglected in the CPW case (the impedance and the propagation speed of the superconducting lines differ less than 1 % with respect to the same values as calculated for normal metal lines). The Libra optimiser was then used for the optimisation of the whole RF design by including normal metal transmission line parameters physically equivalent to superconducting line parameters. The conversion between the two types of transmission lines, was obtained by keeping the width of the lines, their propagation speed and the metal thickness constant, but changing the height of the insulating layer and its dielectric constant to yield the same impedances and propagation velocities of the lines. This method was used to keep the geometry for the computer simulation as close as possible to that of the actual device, so that the program would more correctly

account for discontinuities due to changes in width. The widths and lengths of optimised

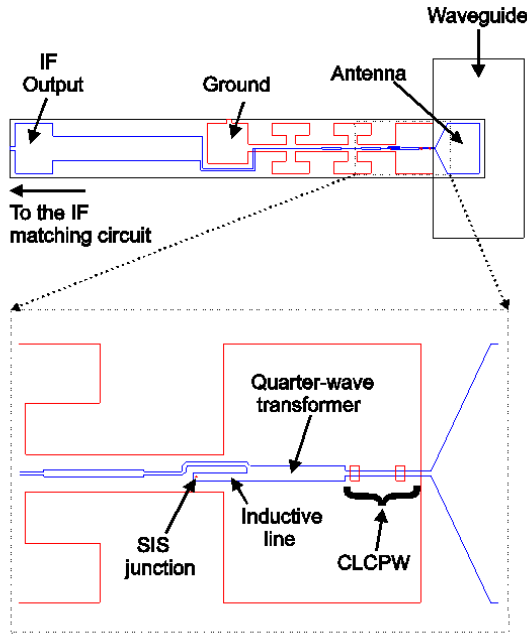


Fig. 7 : Quartz substrate used for the mounting of the SIS junction and the integrated tuning structure. The RF hammer filter is seen in the upper part of the figure. The end-loaded matching structure, including the CLCPW is shown in the bottom.

normal metal microstrip were used to calculate the characteristic impedance and electrical length of the individual sections using Linecalc [12]. A Sonnet [13] model for the effects of discontinuities between coplanar waveguide and microstrip was also included in the Libra model of the mixer chip.

The layout of the whole mixer chip is illustrated in Fig. 7. The upper part of the figure shows the quartz substrate used to support the antenna (on the right) together with the cross section of the waveguide, the RF hammer filter connected to the ground lead, and the IF output (on the left). A detail of the central part of the chip which includes the SIS junction and its integrated matching structure is shown at the bottom of the same figure. The result of simulation of the global structure of the mixer which includes the chip integrated in the mixer block is shown in

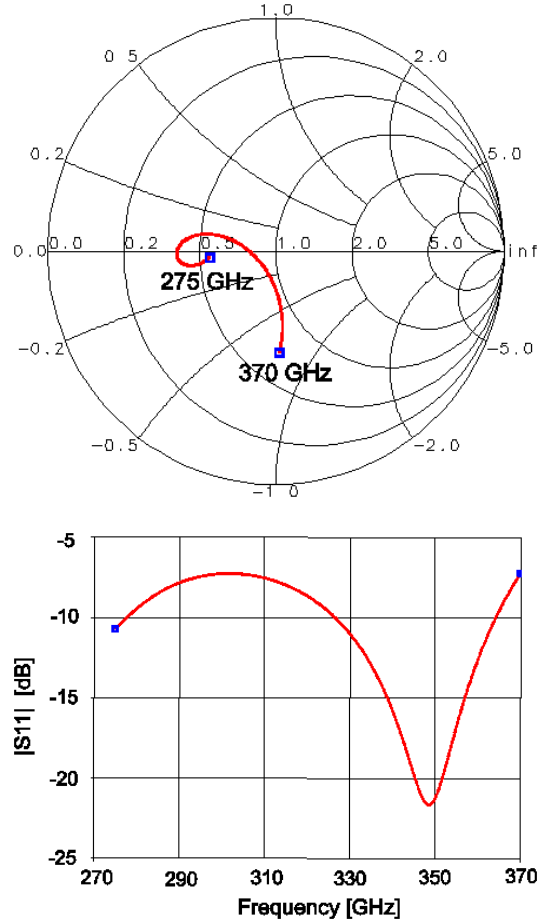


Fig. 8 : On the top : embedding impedance $Z_{emb}(V)$ for the tuned junction in the 275-370 GHz frequency band. The Smith chart is normalised to the RF junction impedance $R_j = 18.7 \text{ W}$. On the bottom : Amplitude of the reflection coefficient $|S11(n)|$ seen at the junction port.

Fig. 8. We can see that a rather a good matching to the RF junction impedance is obtained in the whole frequency band of interest, subject to the constrain that $Z_{emb}(V)$ should remain within the stable region shown on Fig. 6. Thus, this mixer structure fulfils the derived stability criterion and can operate in a wide RF bandwidth.

E. Junction bias and IF matching circuit

To bias the junction and provide IF connection for the IF signal, a narrow microstrip line ($3 \mu\text{m}$) is connected to the first quarter-wave transformer as shown Fig. 7. The connection of this strip to the transformer has been optimised to minimise

the RF leakage through the IF output and guarantee a wide RF bandwidth. This is obtained by using alternating sections of microstrip lines with high and low impedance to increase the impedance ratio at the quarter-wave transformer to IF/bias microstrip transition output.

To allow operations of the mixer into a 50 Ω IF amplifier, an IF matching circuit external to the main mixer block has been designed. For a DSB mixer, a typical value for the real part of the IF output impedance of a SIS junction is of the order of 10 R_n . The junction's IF output is shunted by the parasitic capacitance of the junction and of the RF matching network. The part of the matching network implemented with microstrip uses SiO₂ dielectric between the wire layer and the ground-plane and has a specific capacitance of 0.19 fF/ μm^2 . In our case, the total output capacitance is dominated by the contribution of the tuning circuit and is approximately 800 fF. The output impedance of the mixer includes the quantum reactance and depends on the impedance terminations at the signal and image band. A good compromise between a sufficiently high mixer gain and low SSB mixer noise temperature is obtained by using an IF load impedance of 2-3 times the normal state resistance of the junction [13]. In our case, a value of $2 \cdot R_n = 50 \Omega$ was chosen to allow operation with a 50 Ω LNA with

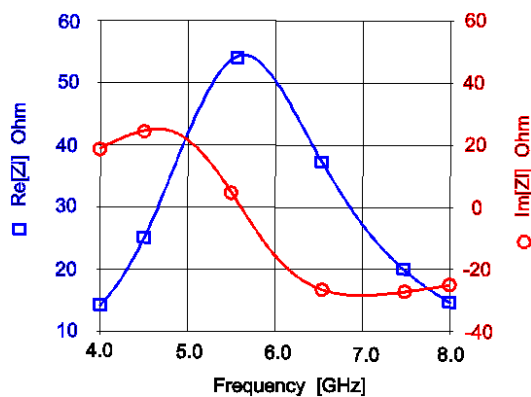


Fig. 9 : IF load impedance Z_l seen by the junction. The IF circuit has been optimised to give a real 50 Ω impedance at the central IF frequency of 6 GHz.

central $\nu_{IF} = 6$ GHz. The IF matching circuit is implemented in a shielded microstrip and is based on an inductive series matching structure, to compensate the IF output capacitance, followed by a 2 sections quarter wavelength Chebishev transformer. In Fig. 9, the real and imaginary parts of the load impedance $Z_l = Y_l^{-1}$ as seen by the junction are plotted in the frequency range between 4 GHz and 8 GHz. The matching circuit has been optimised to give a real 50 Ω impedance at the central IF frequency of 6 GHz. We can see that $\text{Re}[Z_l] > R_n$ over a bandwidth wider than 2 GHz.

F. Gain and mixer noise temperature

The mixer gain and noise are calculated from the quantum theory of mixing using a three-port approximation. The SSB coupled mixer gain $G_{\pm 1}$ is defined as the power coupled to the IF load Y_l divided by the power available from an RF source at the signal or image port (1 or -1). It can be expressed in terms of the Z-matrix:

$$G_{\pm 1}(SSB) = 4 \cdot \text{Re}(Y_{\pm 1}) \cdot \text{Re}(Y_0) \cdot |Z_{0 \pm 1}|^2 \quad (2)$$

The DSB coupled gain $G(DSB)$ is defined as the sum of $G_{+1}(SSB)$ and $G_{-1}(SSB)$:

$$G(DSB) = 4 \cdot \text{Re}(Y_0) \cdot \left[\text{Re}(Y_{-1}) \cdot |Z_{0 -1}|^2 + \text{Re}(Y_1) \cdot |Z_{0 1}|^2 \right]$$

We indicate with G_I the coupled mixer gain in the image band and with G_S the coupled mixer gain in the signal band. The coupled gain depends on the bias and pumping voltage conditions and on the terminating admittances at all three relevant frequencies. The mixer noise temperature has two contributions : the shot noise in the junction current and the quantum vacuum fluctuations. The first contribution is generated by fluctuations in the tunneling

current generated by the combination of bias voltage and LO power. The rms expectation value of this current fluctuation has been calculated using the current correlation H-matrix formulation derived by Tucker and Feldman [5]. The second contribution arises from quantisation of the incident radiation field as calculated by Wengler and Woody [15]. The noise power per unit bandwidth at the output of a mixer calculated from the complete quantum mechanical treatment takes the form :

$$\frac{P_N}{B} = \text{Re}(Y_0) \cdot \sum_{m=-1}^1 \sum_{n=-1}^1 Z_{0m} \cdot Z_{0n}^* \cdot H_{mn} + \sum_{m=-1}^1 G_m \cdot \frac{1}{2} \cdot h \cdot \mathbf{n}_m \quad (3)$$

where H_{mn} is the current correlation matrix, G_m is the coupled conversion gain from the m th port to the output as defined in eq. (2) and B is the bandwidth of the IF system. The contribution of the second term to the noise power has a minimum of $h \cdot \nu / 2$ per bandwidth at each of the mixer input ports. The SSB mixer noise temperature T_M of the DSB mixer referred to the input is defined as :

$$T_M = \frac{T_{out}}{G_S} = \frac{P_N}{k \cdot G_S \cdot B} \quad (4)$$

where k is Boltzmann's constant. The SSB noise temperature of the receiver consisting of a mixer cascaded with an IF amplifier and referred to the mixer input is :

$$T_{rec} = T_M + \frac{T_{IF}}{G_S} \quad (5)$$

where $T_{IF} = 6$ K is the assumed noise temperature of the amplifier operating at a central IF frequency of 6 GHz. We have used eq. (2), (3), (4) and (5) to compute the coupled SSB mixer gain, the SSB mixer noise temperature and the SSB receiver noise temperature of the designed DSB system. The

chosen operating conditions for the calculated quantities are referred to a bias voltage at the middle of the first photon step and to a LO pumping power such that $\alpha=1$. Figure 10 shows the calculated SSB mixer noise temperature T_M (left scale) and the

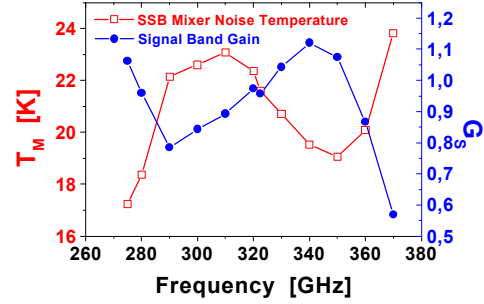


Fig. 10 : SSB mixer noise temperature (left scale) and coupled mixer gain (linear scale) in the signal band G_S (right scale) in the 275-370 GHz frequency band.

coupled SSB signal mixer gain G_S (right scale) of our DSB for a few frequency values in the RF band. The signal band S has been chosen to be the USB or the LSB depending on whether the lower T_{rec} is obtained in USB or LSB. This result shows that the mixer can operate with low mixer noise temperature and high signal conversion gain. Figure 11 shows the result of the calculated SSB receiver noise temperature. We can see that the maximum of $T_{rec} \approx 35$ K (≈ 2 h·v/k) is obtained in the

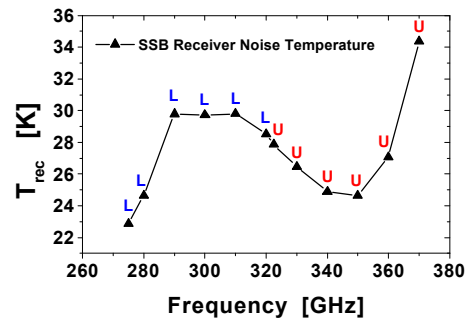


Fig. 11 : Calculated SSB receiver noise temperature referred to the mixer input T_{rec} in the 275-370 GHz frequency band. The letters L and U over each point indicate whether the corresponding T_{rec} value is obtained in LSB (L) or USB (U).

upper part of the RF band. This is due to a simultaneous increase of T_M and of the conversion loss at these frequencies. The result shown in Fig. 10 indicates that a SSB receiver noise temperature as low as $\approx 2\div 3$ times the quantum limit $h\nu/k$ might be achieved in the whole 275-370 GHz frequency band. This receiver noise is referred to the mixer input. The actual value will be degraded due the various elements between the mixer and the measurement plane: LO coupling, waveguide losses, cryogenic windows, refocusing optics. Fig. 12 displays the calculated coupled mixer gain G_S and

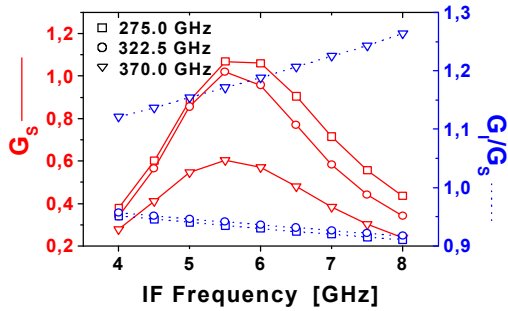


Fig.12: Coupled mixer gain in the signal band G_S (left scale, solid line) and image gain ratio G_I/G_S (right scale, dashed line) in the IF frequency band for three different RF frequencies. Linear scales are used.

image rejection G_I/G_S as a function of frequency in the 4-8 GHz IF band for three different RF frequencies. The maximum signal gain is always obtained close to the 6 GHz IF central frequency and its value rapidly

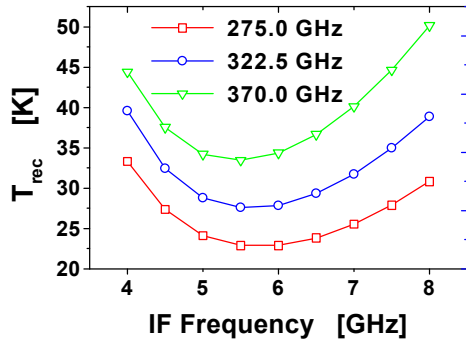


Fig. 13: SSB receiver noise temperature as a function of IF frequency calculated for three different RF frequencies.

decreases at the edges of the IF band. Fig. 13 shows the SSB receiver noise temperature as a function of the IF frequency calculated for three different RF frequencies. We can see that the minimum noise is obtained at 6 GHz and that its degradation at the edges of the IF band is at most 50 % with respect to its value at the central IF frequency.

G. Mixer block construction

The main mixer block is split in two parts that has been made of brass to allow easy machining. The mixer block includes magnetic field concentrators for the suppression of the Josephson current. The whole device is illustrated in Fig. 14. Here the two main parts of the mixer are shown together with the shielded microstrip used as IF matching transformer. The main mixer block has external dimensions $25 \times 20 \times 20$ mm³. The back side of the mixer includes one short section of rectangular waveguide which will be realised with standard micromachining techniques. This part of the mixer block is used for SIS junction mounting. The front part of the main mixer block includes a 10 mm long rectangular waveguide which has been realised by spark erosion technique.

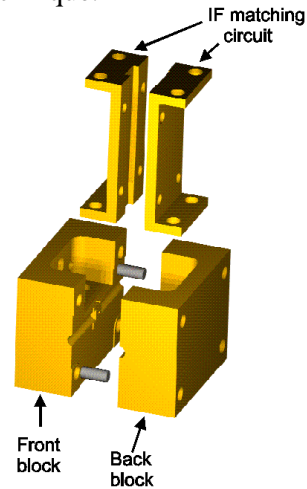


Fig. 14 : Mixer block configuration : the two main parts of the mixer used for the SIS junction mounting are shown together with the shielded microstrip used as IF matching transformer to a 50 W amplifier.

III. SSB mixer

There is a strong interest in the millimetre and submillimetre astronomical community to operate low noise quasi-particle mixers in SSB mode in order to eliminate atmospheric noise in the image band during spectral line observations. In this section we will discuss the design and optimisation of a SSB receiver. The SSB mixer is based on the full-height waveguide to suspended microstrip transition discussed in section II.A (antenna type 2 is used) and on the RF filter described in section II. The main differences between the SSB and DSB mixers are: a) the use of a circular backshort; b) the use of different RF and IF matching circuit.

A. Circular cross section backshort

A mechanically rugged noncontacting backshort with circular cross section has been adopted to provide a large reflection of RF power inside a circular waveguide. The backshort is used for rejection of the image band. Fig. 15 shows the whole backshort unit with a four sections choke. The sliding metallic backshort can be moved in a 880 μm diameter circular waveguide. Its dimensions have been optimised to give best performances in the 275-370 GHz frequency band. We obtain an amplitude of the

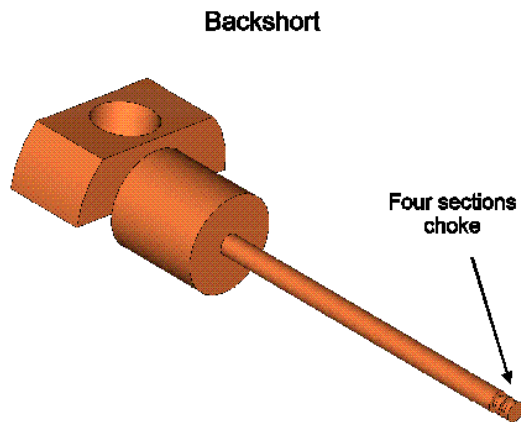


Fig. 15: Circular section non-contacting backshort used for image rejection. A four sections choke-type transformer is used to give large reflection of RF power inside a circular waveguide.

reflection coefficient better than -0.1 dB over the whole bandwidth even when taking into account a 10 μm off-axis displacement with respect to the waveguide axis (mechanical tolerance for off-axis displacement).

Impedance	Diameter	Length
Low	800 mm	200 mm
High	500 mm	240 mm

Tab. 1: Dimensions of low and high impedance sections of the choke.

A conical tapering has been optimised to decrease the reflected power at the transition between the circular waveguide, hosting the backshort, and the rectangular waveguide where the suspended substrate microstrip is located (Fig. 16). Fig. 17 shows the amplitude of the reflection coefficient due to the transition in the 200-400 GHz frequency range, with and without the conical tapered length. With lossless conductors and for narrow band applications, the mismatch at the rectangular/circular transition would not be objectionable, because arbitrary values of the reflection phase seen from the rectangular waveguide can be realised by a suitable position of the circular backshort.

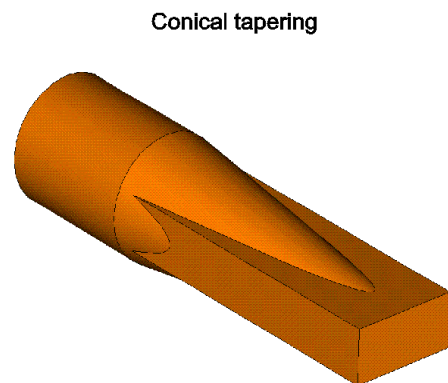


Fig. 16: Circular to rectangular waveguide conical tapering.

However, for our application, this would have the following drawbacks: a) standing

waves between the backshort and the transition increase the stored energy and therefore the losses; b) the tuning curve, i.e. the relation between frequency and reflected phase, would be uneven, leading to irregular spacing between matched and rejected frequencies. Accordingly, we decided to

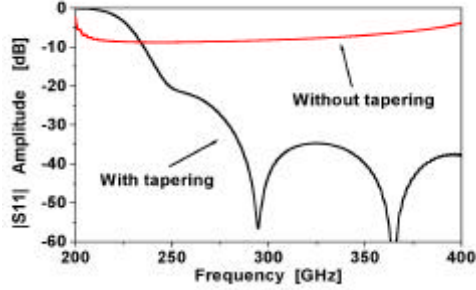


Fig. 17: Amplitude of the reflection coefficient at the circular to rectangular waveguide transition with and without conical tapered section as a function of frequency.

implement a smooth transition between the circular and rectangular cross-sections, and to determine the minimum length of that transition (1.5 mm) to obtain an acceptable match over the operating frequency range.

B. SSB tuning

Fig. 18 shows the configuration of the SSB mixer. The four sections choke-type circular section backshort is used for image rejection. This is realised by selecting a backshort position such that its impedance seen in the probe plane is (approximately) an open at the signal frequency, and a short at the image frequency. RF leakage through IF output is prevented by the optimised six sections RF hammer type filter discussed in the previous section. Figure 19 shows the result of electromagnetic simulations for the calculated input impedance of the probe $Z_p(v)$ of the mixer in Fig. 18 (Ant. 2 geometry reported in Sec. II is used). Again, the input impedance is the driving point impedance between the tip of the probe and the base of the first filter section located on the prolongation of the waveguide wall. The impedance is plotted in a Smith chart and corresponds to a

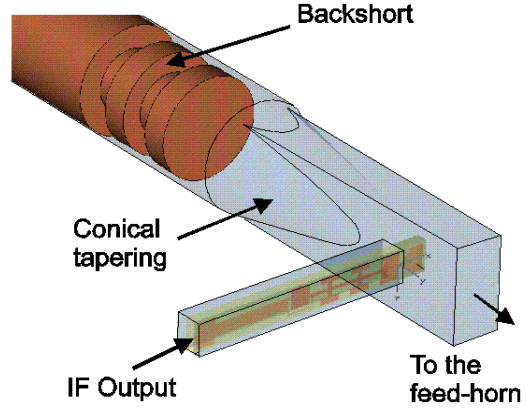


Fig. 18: Full height waveguide SSB mixer. The circular section backshort is used for image rejection.

backshort position l_{bs} located 8 mm away from the antenna plane ($8 \text{ mm} \approx 30 \lambda_g$ at 322.5 GHz). We can see that as the frequency is increased from 275 GHz to 370 GHz, the complex impedance turns in a clockwise manner in the upper part of the chart tracking open circles which periodically pass through the same real

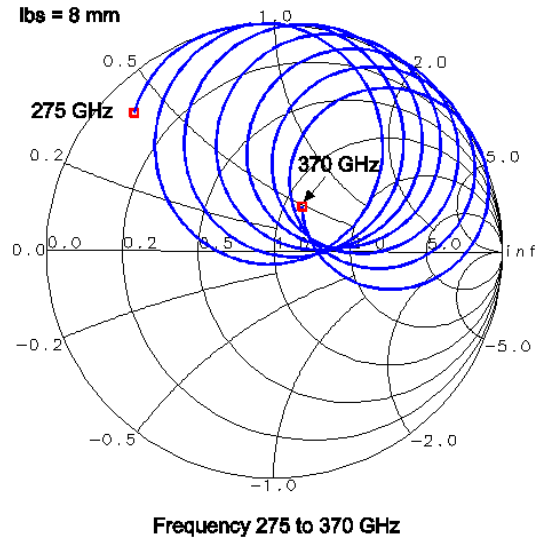


Fig. 19: Input impedance of Ant. 2 probe in suspended microstrip line for the mixer geometry shown in Fig. 18: the circular section backshort is located at a distance $l_{bs}=8\text{mm}$ away from the antenna plane. The Smith chart is normalised to 50 Ω .

impedance value of $Z_C \approx 75 \Omega$. This periodicity is directly related to the value of l_{bs} : the larger l_{bs} , the higher the number of

turns of $Z_P(v)$ in the Smith chart and vice versa. On the other hand, the overall dispersion of the represented $Z_P(v)$ in the above chart does not depend on the chosen value of l_{bs} .

When the antenna 1 probe geometry (discussed in section II) is used instead of antenna 2 with the same l_{bs} value, all open circles periodically get through a real impedance value of $Z_C \approx \text{Re}[Z_C] \approx 50 \Omega$. The antenna probe geometry can be optimised to give a complex impedance with capacitive or inductive or purely real impedance Z_C , and with a dispersion of its $Z_P(v)$ points on the Smith chart as low as possible. The lowest real impedance probe would seem to be more suited to the coupling of low impedance devices as SIS junctions because, ideally, one would like to have an antenna with a low $\text{Re}[Z_C]$ to match directly the low value of the inductively tuned RF impedance of the junction in parallel with its geometric capacitance. A real Z_C value as low as $\approx 35 \Omega$ can be obtained by properly choosing the antenna parameters, i.e. the value of Z_C only depends on the used probe geometry. However, we have found that the lower is Z_C the bigger is the dispersion of the $Z_P(v)$ points in the Smith chart. Therefore a purely real 75Ω probe (ant. 2) has been preferred to lower impedance one for reasons of stability of the receiver which will be explained in next sections.

C. Stability of SSB mixer

Using the Tucker and Feldmann results discussed in section II.C we have derived a stability criterion for a SSB mixer operating in the 275-370 GHz frequency range in the limit of low v_{IF} frequencies ($v_{IF}/v_{LO} \rightarrow 0$). Mixer properties are calculated in the three-port approximation. In a SSB mixer where termination admittances at the signal (Y_S) and image (Y_I) band are different, the real part of the complex IF output admittance (Y_{IF}) can easily become negative if the impedance in the image band is not properly chosen. The IF load admittance Y_I should then be carefully

chosen in such a way that $\text{Re}[Y_{IF}] + \text{Re}[Y_I] > 0$, which is the condition to avoid oscillation. An alternative with better safety margins to this rule which could be adopted to guarantee stable operations would then be to design the SSB mixer by selecting Z_I and the operating conditions for the bias and pumping voltages so that $\text{Re}[Y_{IF}] > 0$ for a value of Z_S giving optimum receiver performances [7]. Here, we have assumed these optimum conditions are reached for a bias voltage V_{DC} at the half of the first photon step, $V_{DC} = V_g - hv_{LO}/2e$, and for a LO pumping voltage parameter $\alpha=1$. Moreover, we have assumed Z_S to match the normal-state resistance of the junction R_n , $Z_S = R_n$, and Z_I to be purely reactive ($Z_I = j \cdot X$ with X arbitrary reactance) which implies that the image band is completely rejected. With the same analytic fit to a good quality I-V curve as the one used in deriving the results of section II.C, we have used a three-frequency approximation to the quantum theory of mixing to constrain the Z_I values necessary to obtain $\text{Re}[Y_{IF}] > 0$ at 322.5 GHz. The resulting values of Z_I normalised to the normal-state resistance fall in the range :

$$-j \cdot 5.14 \leq \frac{Z_I}{R_n} \leq +j \cdot 0.18 \quad (6)$$

and are independent on the R_n value. This condition for the termination impedance in the image band Z_I has been used as a design rule to be fulfilled by the SSB mixer as a first attempt to guarantee stable operations at 322.5 GHz. When the same simulations are repeated in the 275-370 GHz range we find that the lower frequency constrains the limits of the "stability region" :

$$-j \cdot 3.27 \leq \frac{Z_I}{R_n} \leq +j \cdot 0.12 \quad (7)$$

The stability regions derived in eqs. (6) and (7) are plotted in Fig. 20 in a Smith chart normalised to R_n . We can see

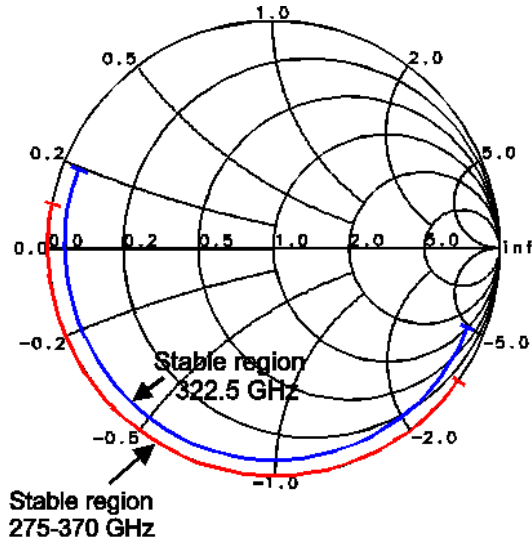


Fig. 20 : "Stability regions" for a purely SSB mixer at 322.5 GHz and in the frequency band 275-370 GHz. The regions indicate the values of $Z_I = jX$ such that $\text{Re}[Y_{IF}] > 0$ for typical operating conditions $\alpha=1$ and $V_{DC} = V_g - h\nu_{LO}/2e$. The Smith chart is normalised to $Z_S = R_n$.

that a positive value for the real part of the IF admittance is obtained by placing Z_S at the centre of the chart (matching), and Z_I in a region which is approximately located in the lower part of the external circle of the chart itself.

D. RF matching circuit

In this section, we first show why we could not use for the SSB mixer the same RF matching circuit as for the DSB mixer. We then describe the solution adopted for the SSB mixer.

The RF impedance of the junction is approximated as an R_j resistance of 18.7Ω in parallel with a 75 fF capacitance (see section II.D). The RF junction impedance in parallel with its capacitance must be transformed to the value of the antenna probe impedance of $\approx 75 \Omega$ (antenna type 2 discussed in sec. II.A is used). The real part of the RF equivalent impedance of the junction ($\approx 2.3 \Omega$) is transformed to the 75Ω antenna probe impedance by means of a series inductive line followed by a two-section quarter-wave Chebyshev transformer similar to the one

shown in Fig. 7 and described in section II.D. The circuit has been optimised as previously discussed by using commercial softwares. The Smith chart (Fig. 21) shows the embedding impedance $Z_{emb}(\nu)$ in the 275-370 GHz frequency band for a backshort position $l_{bs} = 8 \text{ mm}$ away from the antenna plane. A good matching to the junction is obtained at evenly spread intervals in the whole frequency band of interest. The backshort position can be chosen so that a purely reactive impedance $Z_{emb}(\nu_I) = jX_{emb}$ is seen by the junction at a ν_I frequency (image band) which differs by $2 \cdot \nu_{IF} = 12 \text{ GHz}$ from the closest ν_S frequency (signal band) where a matching to the RF junction impedance is obtained. The LO signal is injected at a frequency $\nu_{LO} = (\nu_I + \nu_S)/2$. Either USB or LSB operation can be chosen, for a given signal frequency ν_S , by suitably setting ν_{LO} . Figure 21 shows that, over the frequency range from 275 GHz to 370 GHz, the impedance points are spread out over the whole Smith chart. In particular, a total reflection of the image band is obtained in the upper

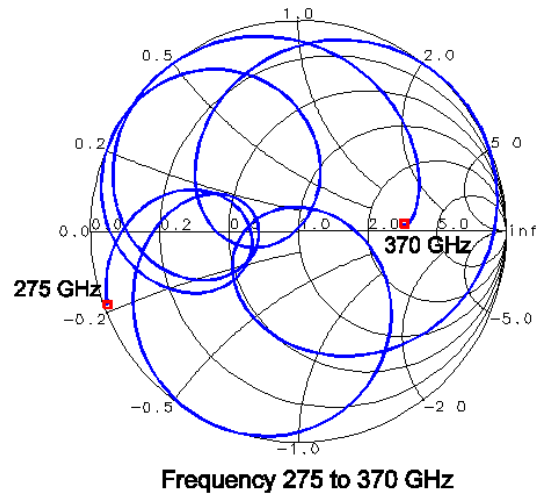


Fig. 21 : Embedding impedance $Z_{emb}(\nu)$ seen by the junction in the 275-370 GHz frequency band. The junction capacitance is tuned out by means of an end-loaded stub (the junction capacitance is considered as part of the embedding circuit). The backshort position is 8 mm away from the antenna plane. The Smith chart is normalised to the RF junction impedance $R_j = 18.7 \Omega$.

part of the external circle of the chart where the previously derived stability criteria of eq. (7) is not met. The spreading of the embedding impedance in the image band is due to the use of a two sections quarter wavelength Chebishev transformer and the approximately $\lambda/8$ long inductive line, causing a rotation of the phase of the reflection coefficient at v_i into the part of the Smith chart corresponding to unstable operations.

A better control of this impedance is obtained by using a lower value for the electrical length between the antenna probe and the junction. This is achieved by adopting a parallel inductive tuning. The required transformation ratio is smaller and can be achieved with a single section $\lambda/4$ transformer. The parallel inductive tuning is achieved with a short ($\approx \lambda/8$) length of microstrip terminated to a virtual ground provided by a radial stub (opening angle 130°). This is shown in Fig. 22 which illustrates the layout of the mixer chip actually used. Over the operating band, the radial stub provides an imaginary

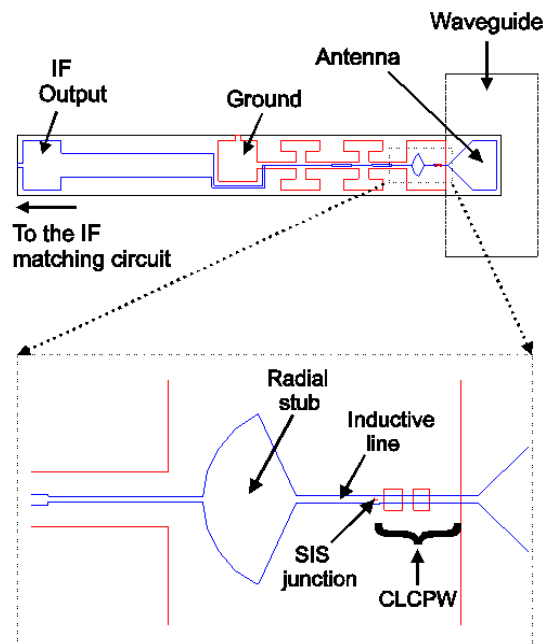


Fig. 22 : Quartz substrate used for the mounting of the SIS junction and the integrated tuning structure. The RF hammer filter is seen in the upper part of the figure. The open-ended matching structure, including the radial stub and the inductive line is shown in the bottom.

impedance with $|\text{Im}[Z_{\text{stub}}(v)]| \leq 0.8 \Omega$. We found, using simulations [13], that, with respect to the conflicting requirements of lowest impedance at the apex on one hand, and minimum capacitive loading of the IF on the other hand, a radial stub offers no clear advantage over a $\lambda/4$ low-impedance rectangular stub. The parallel tuned junction presents, at the centre of the RF band, a real impedance $R_j \approx 18.7 \Omega$ as discussed above. This is matched to the $\approx 75 \Omega$ driving point impedance of the probe by a $\lambda/4$ line with an impedance $Z_L \approx 35 \Omega$. This falls between the impedances that can be realised in, respectively, microstrip and coplanar superconductive lines. Therefore, we have realised this $\lambda/4$ section in CLCPW, consisting of 3 sections of microstrip and 2 sections of coplanar lines. The lengths of the individual sections were optimised, taking into account the actual impedances across the RF band of the inductively tuned junction and of the probe, while ensuring at the same time that the stability criterion for SSB operation was met. Sonnet was used to compute de-embedded S-parameters for the microstrip-coplanar discontinuities, which were used in the Libra simulation of the global circuit. The final result of the optimisation is shown in Fig. 23.

E. Junction bias and IF matching circuit

To bias the junction and provide a path for the IF signal, a narrow microstrip line ($3 \mu\text{m}$) is connected to the external part of the radial stub as shown in Fig. 22. The connection of this strip to the radial stub has been optimised to minimise the RF leakage through the IF output and guarantee a wide RF bandwidth. This is obtained, in a similar way to what previously discussed in section II.E, by using alternating sections of microstrip lines (shown in the upper part of Fig. 22) with high and low impedance to increase the impedance ratio at the radial stub to microstrip transition. To allow operations of the mixer in a 50Ω IF

amplifier, an IF matching circuit external to the main mixer block has been designed. With a specific capacitance of the RF matching network of $0.19 \text{ fF}/\mu\text{m}^2$, and a 75 fF junction capacitance, the total output capacitance of the mixer is dominated by the contribution of the tuning circuit and is of the order of 1 pF . The output impedance of the mixer includes the quantum reactance and depends on the impedance terminations at the signal and image band. An IF load impedance of $2 \cdot R_n = 50 \ \Omega$ was chosen to allow operation with the LNA operating with central frequency $\nu_{\text{IF}} = 6 \text{ GHz}$.

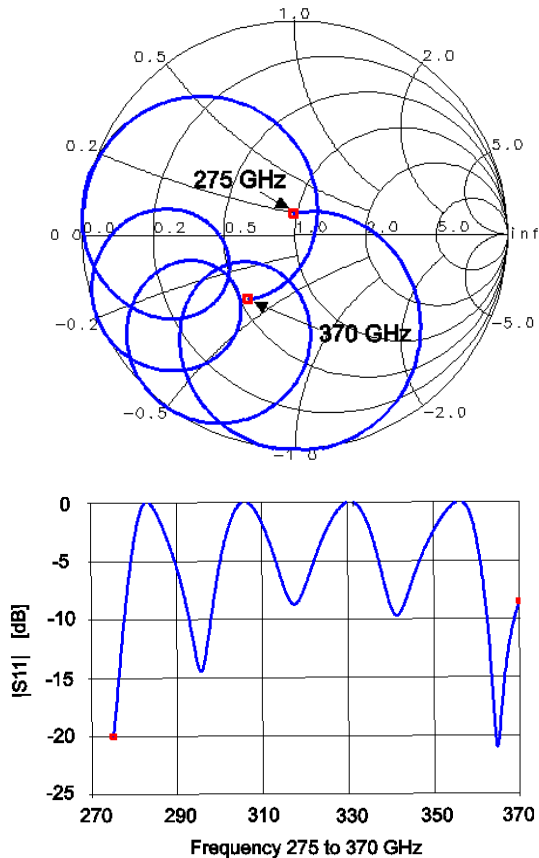


Fig. 23 : Junction capacitance tuned out with an open-ended stub. The backshort is located 4 mm away from the antenna plane. On the top : embedding impedance $Z_{\text{emb}}(\nu)$ in the $275\text{-}370 \text{ GHz}$ frequency band. The Smith chart is normalised to the RF junction impedance $R_j = 18.7 \ \Omega$. On the bottom : Amplitude of the reflection coefficient $|S_{11}(\nu)|$ seen by the junction.

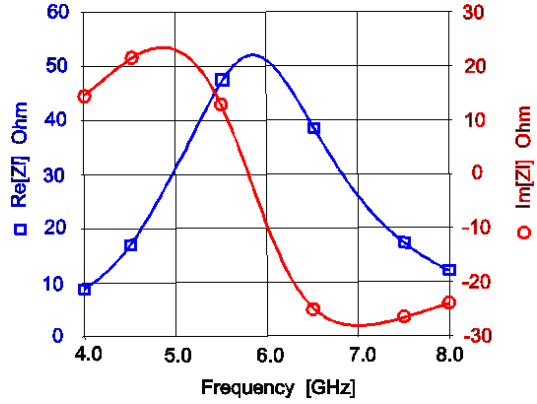


Fig. 24 : IF load impedance Z_l seen by the junction. The IF circuit has been optimised to give a real impedance of $50 \ \Omega$ at the central IF frequency of 6 GHz .

The IF matching circuit is implemented in a shielded microstrip and is based on a 2 sections quarter wavelength Chebisev transformer followed by a $50 \ \Omega$ line directly connected to a SMA. In Fig. 24, the real and imaginary parts of the load impedance $Z_l = Y_l^{-1}$ as seen by the junction are plotted in the frequency range between 4 GHz and 8 GHz . We can see that $\text{Re}[Z_l] > R_n$ over a bandwidth wider than 2 GHz .

F. Gain and mixer noise temperature

We have used eq. (2), (3), (4) and (5) of section II.F to compute the coupled mixer gain, the image band rejection, the SSB mixer noise temperature and the SSB receiver noise temperature of our SSB receiver. The chosen operating conditions for the calculated quantities refer to a bias voltage at the half of the first photon step and to a LO pumping power such that $\alpha=1$. The receiver has been optimised for SSB operations by tuning the backshort distance from the antenna plane l_{bs} to allow operations with low G_I/G_S in either USB or LSB at each frequency in the RF band. Fig. 25 shows the estimated SSB mixer noise temperature T_M (left scale) and the coupled signal gain G_S (right scale) of our mixer.

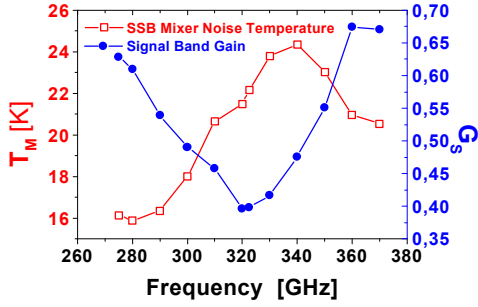


Fig. 25 : SSB mixer noise temperature and coupled mixer gain in the signal band G_s (linear scale) in the 275-370 GHz frequency band.

This result shows that the mixer can operate with low mixer noise temperature and reasonable signal conversion gain. Fig. 26 shows the result of the calculated SSB receiver noise temperature at the mixer input flange and the backshort to antenna plane distance l_{bs} expressed in mm required for the SSB tuning. We can see that the maximum of $T_{rec} \approx 38$ K (≈ 2.4 h-v/k) is obtained at 330 GHz with a tuning in USB obtained with a backshort placed ≈ 4.3 mm away from the junction plane. The result reported in Fig. 26 shows that a SSB receiver noise temperature, referred to the mixer input, as low as $\approx 2\div 3$ times the quantum limit h-v/k could be achieved in the whole 275-370 GHz frequency band. The actual value will be degraded due to various elements between the mixer and the measurement plane as

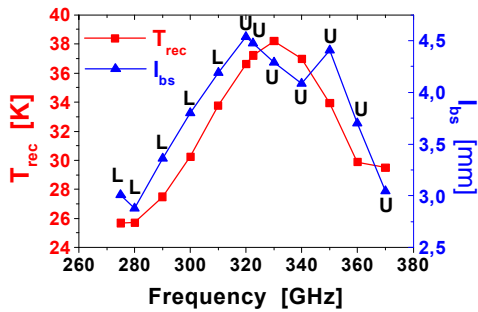


Fig. 26 : Calculated SSB receiver noise temperature referred to the mixer input T_{rec} (left scale) and backshort distance to the antenna plane l_{bs} (right scale) in the 275-370 GHz frequency band. The letters L and U reported over each l_{bs} point indicate whether the optimised performances for the SSB tuning are obtained in LSB (L) or USB (U).

discussed in section I. Fig. 27 shows the variation of the coupled signal gain and image rejection as a function of IF frequency in the 4-8 GHz band for three different RF frequencies. We can see that an image rejection better than -8.5 dB is obtained in a 4 GHz IF band. Fig. 28 shows the SSB receiver noise temperature as a function of IF frequency for three different RF frequencies. We can notice that, except for the case of RF tuning at 370 GHz,

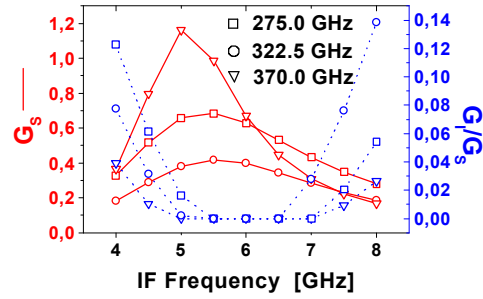


Fig. 27: Coupled signal gain (left scale) and image rejection (right scale) as a function of IF frequency for three different RF frequencies. Linear scales are used.

the increase of the noise temperature at the edges of the band is less than 50 % of the value of the noise at the central IF frequency of 6 GHz.

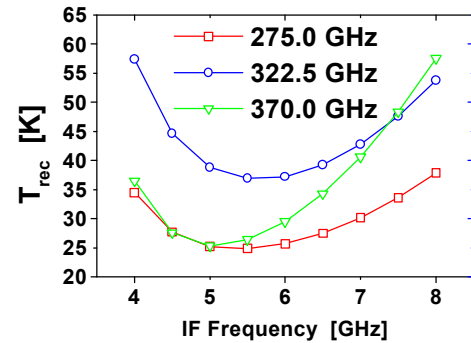


Fig. 28: SSB receiver noise temperature as a function of IF frequency for three different RF frequencies.

G. Mixer block construction

The main mixer block is split in two parts which have been made out of brass allow easy machining. The mixer block includes magnetic field concentrators for the suppression of the Josephson current. The whole device is illustrated in Fig. 29. Here the two main parts of the mixer are shown together with the circular section backshort and the shielded microstrip used as IF matching transformer. The main mixer block has external dimensions $25 \times 20 \times 25 \text{ mm}^3$.

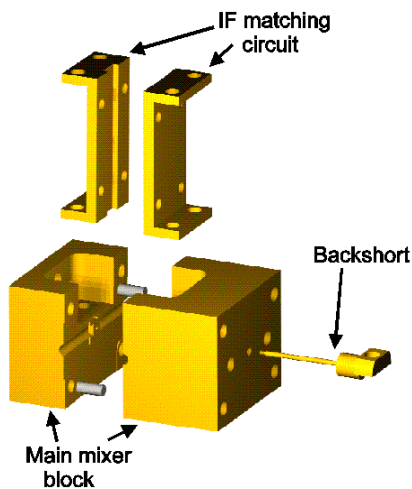


Fig. 29 : Mixer block configuration : the two main parts of the mixer used for the SIS junction mounting are shown together with the circular section backshort and the shielded microstrip used as IF matching transformer to a 50 Ω amplifier.

One part of the mixer includes the circular waveguide, housing the backshort, the conical transition from circular to rectangular waveguide, and a short section of rectangular waveguide. This part of the mixer is used for SIS junction mounting. The other part of the main block includes a 10 mm long rectangular waveguide which will be realised by spark erosion technique and is identical to the one used for the DSB mixer discussed in section II.G. The other parts of the block will be micromachined in a standard way.

IV. Conclusions

Two new types of SIS heterodyne quasi-particle mixers, a DSB and a SSB, have been designed for the 275-370 GHz band. Both mixers employ a tuned junction mounted in a full height waveguide. A "hammer" type filter is used to prevent RF signal leakage through the IF and DC connections to the junction. The mixers and its external circuit have been optimised to give wide RF bandwidth, stable operation, low mixer noise temperature and adequate gain. The RF matching network of the DSB mixer consists of an end-loaded stub followed by two quarter-wave transformer one of which is realised in CLCPW. SSB receiver noise temperatures referred to the mixer input in the range 23-35 K are expected in the RF band with a mixer conversion gain better than -2.5 dB . The RF tuning circuit of the SSB mixer consists of an open-ended stub including a radial stub and an inductive microstrip line. A CLCPW line is used either for the matching of the RF junction impedance to the antenna impedance or to assure stable operations. A circular cross-section backshort can be moved inside a circular waveguide and it is used for the rejection of the image band. SSB receiver noise temperature in the range 25-38 K are expected in the RF band with mixer conversion gain better than -4 dB . The IF matching circuits of both mixers are realised in shielded microstrips to allow operation in a 50Ω LNA operating in the 4-8 GHz frequency band with a central IF frequency of 6 GHz.

Acknowledgements

The authors are grateful to D. Billon-Pierron, M. Carter, F. Mattiocco, I. Peron, K.F. Schuster for helpful discussion. This work was supported in part by the Institut de Radio Astronomie Millimétrique IRAM

(Grenoble, France), and by the CNAO, Astrophysical Observatory of Arcetri (Florence, Italy).

References

¹G. Yassin and S. Withington, "Analytical Expression for the Input Impedance of a Microstrip Probe in Waveguide", *Int. J. Infrared and Millimetre Waves*, **17**, 1685-1705, 1996

²CST Microwave Studio, BÜdinger Str. 2 a, D-64289 Darmstadt, Germany

³I.P. Polichronakis and S.S. Kouris, "Higher Order Modes in Suspended Substrate Microstrip Lines", *IEEE Trans. Microwave Theory and Techniques*, **41**, (8), 1449-1454, 1993

⁴J.R. Tucker, "Quantum limited detection in tunnel junction mixers", *IEEE J. Quantum Electron.*, **6**, 1234-1258, 1979

⁵J.R. Tucker and M.J. Feldman, "Quantum detection at millimetre wavelengths", *Rev. Mod. Phys.*, **57**, 1055-1113, 1985

⁶S.-K. Pan and A.R. Kerr, "SIS mixer analysis with non-zero intermediate frequencies", *Seventh International Symposium on Space Terahertz Technology*, Charlottesville, March, 1996

⁷L. D'Addario, "Noise Parameters of SIS Mixers", *IEEE Trans. Microwave Theory and Techniques*, **36**, (7), 1196-1206, 1988

⁸K.-F. Schuster, IRAM Technical Memo, 1998

⁹T.H. Büttgenbach, H.G. LeDuc, P.D. Maker, T.G. Phillips, "A Fixed Tuned Broadband Matching Structure for Submillimetre Astronomy", *IEEE Trans. Applied Supercond.*, **2**, (3), 165-175, 1992

¹⁰J.W. Kooi, M. Chan, B.Bumble, H.G. LeDuc, P.L. Schaffer, T.G. Phillips, "180-425 GHz low noise SIS waveguide receivers employing tuned Nb/AlO_x/Nb tunnel junctions", *Int. J. Infrared and Millimetre Waves*, **15**, (5), 1994

¹¹W.M. Chang, "The inductance of a superconducting strip transmission line", *J. Appl. Phys.*, **50**, 8129-8134, 1979

¹²Touchstone CAD Software, EEsof, Westlake Village, CA

¹³Sonnet Software, Inc., 1020 Seventh North Street, Suite 210, Liverpool, NY 13088, USA

¹⁴J.W. Kooi, F. Rice, G. Chattopadhyay, S. Sundarum, S. Weinreb, T.G. Phillips, "Regarding the IF output conductance of SIS tunnel junctions and the integration with cryogenic InP MMIC amplifiers", *Tenth International Symposium on Space Terahertz Technology*, Charlottesville, 1999

¹⁵M.J. Wengler, D.P. Woody, "Quantum noise in heterodyne detection", *IEEE J. Quantum Electron.*, **23**, 613-622, 1987